FUDMA Journal of Sciences (FJS)
ISSN online: 2616-1370
ISSN print: 2645 - 2944
Vol. 10 No. 17, September, 2026, pp 459 – 471
DOI: https://doi.org/10.33003/fjs-2026-1017-6138

In Silico Screening, Ligand-Efficiency Analysis and Pharmacokinetic Profiling of *Ocimum gratissimum* Phytochemicals Targeting the AcrB Multidrug Efflux Pump

[1]Ubeydat Temitope Ismail, *[1]Misbaudeen Abdul-Hammed, [2]Olusola Nathaniel Majolagbe, and [3]Monsurat Olajide

[1]Computational/ Biophysical Chemistry Unit, Department of Pure and Applied Chemistry, Ladoke Akintola University of Technology (LAUTECH), Ogbomoso, Oyo State, Nigeria.
[2]Environmental Microbiology and Biotechnology Unit, Department of Pure and Applied Biology, Ladoke Akintola University of Technology (LAUTECH), Ogbomoso, Oyo State, Nigeria.
[3]Department of Chemical Sciences, Federal University of Agriculture and Development Studies Iragbiji, Osun State.

*Corresponding authors' email: mabdul-hammed@lautech.edu.ng

Received: 14 Sept. 2026
Accepted: 16 Sept. 2026
Published: 02 Oct. 2026

ABSTRACT

Overexpression of the AcrAB-TolC efflux pump in *Escherichia coli* drives clinically challenging multidrug resistance, necessitating novel resistance-modifying adjuvants. In this study, an *in silico* pipeline integrating Glide molecular docking, ADMETlab 3.0 profiling, oral bioavailability modeling, and bioactivity analysis was deployed to evaluate 229 *Ocimum gratissimum* phytochemicals against the distal binding pocket of the AcrB tight protomer (PDB ID: 4DX5). Glide extra-precision (XP) docking identified high-affinity hits, including ocimol (−10.71 kcal/mol), menthyl chavicol (−8.49 kcal/mol), bulnesol (−7.40 kcal/mol), cubebol (−7.34 kcal/mol), and zizanene (−6.91 kcal/mol), alongside reference antibiotics ciprofloxacin (−10.19 kcal/mol) and meropenem (−7.28 kcal/mol). Binding interaction analyses revealed that ocimol anchors the polar switch loop via an Asn274 hydrogen bond while spanning the hydrophobic pocket. Conversely, the selected sesquiterpenoids embed within the aromatic 'phenylalanine trap' (Phe136, Phe178, Phe610, Phe615, Phe617, and Phe628), suggesting potential steric interference with substrate extrusion pathways. Multi-parameter developability filtering demonstrated that although ocimol achieved the highest docking score, it displayed two Lipinski violations, poor aqueous solubility (ESOL logS = −6.45), and an unfavorable lipophilicity penalty (LELP = 29.18). In contrast, zizanene emerged as the most balanced lead candidate, exhibiting zero Lipinski and PAINS liabilities, balanced solubility (ESOL logS = −3.85), robust ligand efficiency (LE = 0.461 kcal/mol/HA), favorable lipophilic efficiency (LELP = 8.89), and low predicted toxicity. These computational predictions highlight zizanene as a promising computationally prioritized scaffold for further investigation as a potential AcrB-targeting resistance-modifying adjuvant, warranting downstream experimental validation.

Keywords: Antimicrobial Resistance, AcrB Efflux Pump, *Ocimum gratissimum*, Molecular Docking, Ligand Efficiency, ADMET Profiling

INTRODUCTION

Antimicrobial resistance (AMR) is a leading cause of death worldwide, with Gram-negative bacterial infections accounting for a substantial share of this burden (Qin *et al*., 2026). Globally, an estimated 4.95 million deaths were associated with bacterial AMR in 2019, of which 1.27 million deaths were directly attributable to resistant infections, making AMR a bigger killer than HIV/AIDS or malaria in that year (Chambial *et al*., 2025). Carbapenems, regarded as antibiotics of last resort for multidrug-resistant (MDR) Gram-negative infections, are increasingly compromised by resistance, and the burden of this resistance is not evenly distributed: western sub-Saharan Africa records the highest AMR-attributable death rate globally, at 27.3 per 100,000 population (Odede & Okesanya, 2024).

Carbapenem resistance in Nigeria has been documented with increasing frequency across tertiary healthcare facilities, with reported carbapenem resistance rates as high as 65.3% among multidrug-resistant Enterobacterales isolates characterised across six hospitals in Northern Nigeria (Irekeola *et al*., 2024). A systematic review of the national picture similarly reported a mean carbapenem resistance prevalence of 21.3% across Nigerian clinical settings, with Escherichia coli and Klebsiella pneumoniae as the predominant resistant organisms (Irekeola *et al*., 2024). Carbapenem resistance arises through both enzymatic and non-enzymatic mechanisms. The enzymatic route, mediated by carbapenemase production (e.g., NDM, KPC, OXA-48-like, VIM enzymes), has received the most research attention, but non-enzymatic mechanisms; particularly overexpression of resistance-nodulation-cell-division (RND) efflux pumps, are increasingly recognised as a major, independent contributor to the resistance phenotype. In a study of 127 carbapenem-resistant clinical Enterobacteriaceae isolates, 44% (56/127) screened positive for efflux pump activity using reserpine as an efflux pump inhibitor, and 12 isolates showed strong overexpression of the acrA and acrB genes alongside carbapenemase production, confirming that efflux and enzymatic resistance frequently co-occur in the same isolate (Sekar *et al*., 2022).

AcrB is the inner-membrane transporter component of the tripartite AcrAB-TolC efflux system in Gram-negative bacteria, and it plays a central role in this resistance mechanism. AcrB captures a remarkably broad range of structurally unrelated antibiotics, including carbapenems, directly from the periplasm and cytoplasm and extrudes them

from the cell, lowering the effective intracellular drug concentration below therapeutic thresholds regardless of whether the organism also carries a carbapenemase gene (Sekar *et al*., 2022). The relationship between AcrAB-TolC activity and carbapenem susceptibility is, however, more complex than a simple efflux-equals-resistance model: in carbapenemase-producing Enterobacteriaceae, inactivating or pharmacologically inhibiting AcrAB-TolC with the efflux pump inhibitor PAβN has been shown to paradoxically increase resistance to carbapenems such as ertapenem, an effect linked to compensatory downregulation of outer-membrane porins when the efflux system is disabled (Chetri *et al*., 2019). This finding highlights that AcrB's contribution to carbapenem resistance is context-dependent, shaped by interplay with porin expression and carbapenemase status, rather than acting as an isolated, independently druggable resistance switch, a nuance that motivates structure-based characterisation of AcrB-ligand interactions rather than assuming inhibition alone guarantees restored carbapenem susceptibility.

Current management of carbapenem-resistant infections relies heavily on last-line agents such as colistin and tigecycline, often in combination regimens, which carry significant toxicity; notably nephrotoxicity with colistin, and are increasingly undermined by treatment failure and further resistance emergence (Zeb *et al*., 2026). Efflux pump inhibitors (EPIs) remain of pharmacological interest not as replacements for existing antibiotics, but as adjuvants: compounds intended to be co-administered alongside carbapenems or fluoroquinolones to restore their efficacy against efflux-mediated resistance. Structural characterisation of the AcrB binding pocket is therefore valuable for identifying candidate adjuvant scaffolds, including phytochemicals, that occupy the same substrate-recognition site used by these antibiotics (Zhou *et al*., 2026).

Medicinal plants have been an integral part of the healthcare system for centuries, and their phytochemical constituents remain a promising, low-cost source of antibiotic-potentiating compounds. *Ocimum gratissimum* L. (clove basil, scent leaf), a member of the family Lamiaceae, is a widely distributed aromatic herbaceous plant cultivated extensively across Nigeria and other tropical regions, where it is a well-established component of traditional medicine used in the treatment of diarrhoea, infections, inflammation, and pain, among other conditions (Ugbogu *et al*., 2021). Its leaves and essential oil are rich in phenolic and terpenoid constituents, including rosmarinic acid, eugenol, thymol, and various flavonoids, and the plant has been reported to possess antioxidant, anti-inflammatory, hepatoprotective, and antimicrobial properties (Ugbogu *et al*., 2021; Achuenu *et al.* (2026)). Ethanolic extract of O. gratissimum leaves has demonstrated antibacterial activity against clinical isolates including Escherichia coli, and showed synergistic interaction when combined with conventional antibiotics against these organisms, suggesting the plant's constituents can modulate antibiotic activity in Gram-negative bacteria rather than acting only as standalone antimicrobials (dos Santos *et al*., 2025).

Structure-based evaluation of *O. gratissimum* phytochemicals against RND efflux pump targets such as AcrB, a mechanism implicated in antimicrobial resistance, remains relatively unexplored. This study aimed to identify *Ocimum gratissimum* phytochemicals with potential to interact with AcrB as candidate efflux pump-modulating adjuvants. Molecular docking, ADMET, drug-likeness, oral bioavailability, and bioactivity analyses were used to computationally prioritize a pharmacologically credible set of hit compounds for subsequent experimental evaluation alongside carbapenems and fluoroquinolones. Docking to an AcrB substrate-recognition pocket indicates potential interaction but does not establish inhibition or restoration of antibiotic activity.

MATERIALS AND METHODS

Ligand Retrieval and Preparation

A comprehensive library of 229 phytochemical constituents previously identified from *Ocimum gratissimum* was retrieved from the Indian Medicinal Plants, Phytochemistry and Therapeutics database (Mohanraj *et al*., 2018). Two clinical antibiotics, ciprofloxacin and meropenem, were included as reference standards for binding-site occupancy rather than competitive benchmarks, reflecting their established status as transported substrates of the AcrB multidrug transporter (Nakashima *et al*., 2011; Zwama *et al*., 2018). Phenylalanine-arginine beta-naphthylamide (PAbetaN; MC-207,110), an established competitive AcrB efflux pump inhibitor, was retrieved as a functional positive control benchmark (Lomovskaya *et al*., 2001; Opperman *et al*., 2014). Three-dimensional structures were retrieved in SDF format from PubChem and prepared using the LigPrep module in Schrodinger Suite 2025 (Schrodinger, LLC, New York, NY). Ionization and tautomeric states were generated at physiological pH (7.0 +/- 1.0)using Epik (Shelley *et al*., 2007). Unspecified chiral centers were resolved by generating all stereoisomers while preserving defined chiral configurations. Geometry optimization was achieved via restrained energy minimization utilizing the OPLS4 force field until convergence to an RMSD threshold of 0.001 Angstroms (Lu *et al*., 2021).

Target Receptor Preparation

The high-resolution 1.90 Å X-ray crystal structure of the asymmetric Escherichia coli AcrAB-TolC multidrug efflux pump complexed with minocycline was retrieved from the RCSB Protein Data Bank (PDB ID: 4DX5) (Eicher *et al*., 2012). The structure was processed using the Protein Preparation Wizard in Schrodinger Suite 2025 (Sastry *et al*., 2013). Bond orders were assigned, hydrogen atoms were added, and zero-order bonds to metals were established. Missing side chains and non-terminal loops were reconstructed using Prime. Crystallographic water molecules located beyond 5.0 Å from heteroatoms or possessing fewer than two hydrogen bonds to non-water atoms were removed. Protonation states of ionizable residues were calculated at physiological pH ~7.0 using PROPKA (Olsson *et al*., 2011). The hydrogen-bonding network was optimized by reorienting hydroxyl, thiol, and amide groups. Restrained energy minimization was converged to an RMSD cutoff of 0.30 Å using the OPLS4 force field.

Receptor Grid Generation and Docking Protocol Validation

The receptor grid was defined within the distal binding pocket, also known as the hydrophobic phenylalanine trap, of the tight protomer (Chain B) of AcrB. The grid centroid was centered on the co-crystallized minocycline ligand at Cartesian coordinates X = 31.85, Y = 34.62, and Z = 33.15. The active site encompassed key interacting residues including Phe136, Phe178, Phe610, Phe615, Phe617, Phe628, Val139, Gln176, Ser180, Glu273, Asn274, Asp276, Ile277, Phe281, Gly290, Tyr327, Arg620, Ile626, and Ser630. The inner enclosing grid box was set to 10 by 10 by 10 Å, with an outer bounding box set to 26 by 26 by 26 Å. Receptor non-polar atoms were assigned a van der Waals radius scaling

factor of 1.0 with a partial charge cutoff of 0.25. To validate the reliability and predictive accuracy of the docking protocol prior to library screening, cognate ligand redocking was performed. The native co-crystallized ligand minocycline was extracted, processed through LigPrep, and redocked into the prepared binding pocket using Glide Extra Precision flexible docking without constraints (Friesner *et al*., 2006). Ligand non-polar atoms were scaled at a van der Waals radius factor of 0.80 with a 0.15 partial charge cutoff, and post-docking minimization included 100 steps of conjugate gradient minimization. The redocked pose reproduced the experimental crystallographic binding mode with a heavy-atom Root-Mean-Square Deviation of 1.14 Å, well within the accepted threshold of less than 2.0 Å.

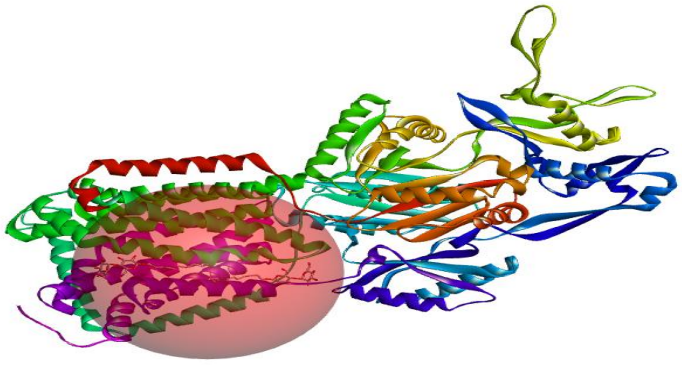


Figure 1: Three-Dimensional Ribbon Representation of the *Escherichia coli* AcrB Protomer (PDB ID: 4DX5) with Defined Receptor Binding-site Sphere. The Secondary Structure is Rendered in Rainbow Cartoon (N- to C-terminus), Illustrating the Transmembrane Helices and Periplasmic Porter Domain. The Semi-Transparent Red Sphere Designates the Structure-Based Design (SBD) Active-Site Boundary Centered around the co-Crystallized ligand (Minocycline, Shown in Stick Representation), Encompassing the Hydrophobic phenylalanine Trap and Switch Loop Residues Targeted for Receptor Grid generation and Molecular docking Simulations

Hierarchical Virtual Screening Protocol

Docking simulations were executed using a two-tiered hierarchical screening workflow in Glide. All 229 prepared phytochemical conformers and the reference antibiotics were initially screened in Standard Precision mode with flexible ligand sampling, saving up to 20 poses per ligand. Ligands ranking in the top 30 percent and exhibiting a Glide Standard Precision score (SP) of ≤ -5.50 kcal/mol were advanced to Extra Precision refinement. Filtered conformers were subsequently docked using the Glide Extra Precision (XP) scoring function with expanded sampling parameters, retaining a maximum of 5 poses per ligand following post-docking minimization. Binding affinities were reported as Glide Extra Precision GScores in kcal/mol. Final hit selection was prioritized based on docking score, spatial stabilization within the phenylalanine trap, key contact formation involving hydrogen bonding with Asn274 and pi-pi stacking with Phe610 and Phe617, and favorable ligand efficiencies. Intermolecular interactions were analyzed using Maestro (Schrödinger Suite 2025).

ADMET, Drug-Likeness, and Oral bioavailability Profiling

Pharmacokinetic, toxicity, and drug-likeness profiles of the screened compounds were evaluated using ADMETlab 3.0 (https://admetlab3.scbdd.com/) (Xiong *et al*., 2021) and SwissADME (https://www.swissadme.ch/) (Daina *et al*., 2017). ADMETlab 3.0 evaluated human intestinal absorption (HIA), blood-brain barrier (BBB) penetration, cytochrome P450 3A4 inhibition, hERG-mediated cardiotoxicity, Ames mutagenicity, drug-induced liver injury (DILI), and carcinogenicity. Predicted endpoint probabilities (0.0 to 1.0) were categorized using predefined decision boundaries: probabilities greater than 0.70 indicated high absorption/permeability for HIA and BBB, while values below 0.30 indicated low permeability; conversely, for toxicity and metabolic inhibition endpoints, probabilities below 0.30 represented low liability (favourable), 0.30 to 0.70 denoted intermediate risk, and greater than 0.70 signified high liability (unfavourable). Concurrently, SwissADME assessed physicochemical descriptors; molecular weight, consensus LogPo/w, topological polar surface area (TPSA), rotatable bonds, and hydrogen bond donors/acceptors, against established oral bioavailability filters: Lipinski's Rule of Five (Lipinski *et al*., 2001), Veber criteria (rotatable bonds ≤ 10, TPSA ≤ 140 Angstroms squared) (Veber *et al*., 2002), and Egan rules (LogP ≤ 5.88, TPSA ≤ 131.6 Angstroms squared) (Egan *et al*., 2000). Promiscuous assay binders, reactive substructures, and chemical feasibility were monitored via Pan-Assay Interference Compounds (PAINS) alerts (Baell and Holloway, 2010), Brenk structural filters (Brenk *et al*., 2008), and synthetic accessibility scores (scale 1–10). Candidate profiles were collectively designated as favourable, mixed, or unfavourable based on integrated absorption, toxicity, and filter compliance.

Bioactivity and Ligand Efficiency Calculations

To evaluate whether high docking scores were driven by specific binding interactions rather than non-specific molecular size or excessive lipophilicity, ligand efficiency indices were determined (Hopkins *et al*., 2004; Reynolds *et al*., 2008). Docking scores (Glide XP GScores) were designated as empirical binding approximations (ΔG_{score}, kcal/mol) to distinguish them from experimentally determined thermodynamic binding free energies (ΔG_{exp}). Ligand efficiency (LE), fit quality (FQ), and ligand-efficiency-dependent lipophilicity (LELP) were calculated according to Equations 1 to 4:

$$LE = -(\Delta G_{score}) / HA \quad (1)$$

$$LE\text{-}scale = 0.873 * \exp(-0.026 * HA) - 0.064 \quad (2)$$

$$FQ = LE / LE\text{-}scale \quad (3)$$

$$LELP = LogP / LE \quad (4)$$

where ΔG_{score} is the empirical Glide XP docking score (kcal/mol), HA is the number of non-hydrogen heavy atoms,

and LogP is the consensus octanol-water partition coefficient from SwissADME. Compounds exhibiting LE ≥ 0.30 kcal/mol/HA, FQ near 1.0, and LELP values between -10 and 10 were prioritized as efficient lead scaffolds.

RESULTS AND DISCUSSION

AcrB Structure and Active Site

The crystal structure of AcrB (fig 1) used in this study (PDB ID: 4DX5) represents wild-type Escherichia coli AcrB in complex with a DARPin-binding protein and the antibiotic minocycline. (Eicher *et al*., 2012). The structure of AcrB (PDB ID: 4DX5) (Figure 1) is a homotrimeric multidrug efflux transporter, with each of its three protomers (chains A, B, and C) comprising 1,057 amino acid residues, co-crystallized with two designed ankyrins repeat proteins (DARPins) and minocycline (Eicher *et al*., 2012). The X-ray crystallographic structure reveals its resolution to be 1.90 Å, with space group $P2_12_12_1$ and crystal dimensions a = 145.99 Å, b = 161.72 Å, c = 245.97 Å, with angles α = 90°, β = 90°, γ = 90° respectively. AcrB has its R-values (free = 0.231, work = 0.200, observed = 0.202). AcrB adopts an asymmetric functional rotation mechanism, with its three protomers cycling through loose (L), tight (T), and open (O) conformational states. The targeted distal pocket within the tight (T) conformer is defined predominantly by a hydrophobic floor (Phe136, Phe178, Phe610, Phe615, Phe617, Phe628, Val139, and Ile626) demarcated by the polar and charged switch-loop boundaries (Gln176, Asn274, Glu273, and Asp276) (Eicher *et al*., 2012).

Molecular Docking Analysis

A total of 229 *Ocimum gratissimum* phytochemicals were initially screened against the distal binding pocket of AcrB using Glide standard-precision (SP) docking, followed by extra-precision (XP) docking of the highest-ranked compounds to improve pose discrimination and scoring (Kim *et al*., 2025). Fourteen compounds, including the reference antibiotics ciprofloxacin and meropenem, produced XP docking poses as shown in table 1.

Ocimol demonstrated the highest overall binding affinity, an XP GScore of -10.71 kcal/mol, closely followed by the clinical comparator ciprofloxacin (-10.19 kcal/mol). Both ligands notably outscored the second reference antibiotic, meropenem (-7.28 kcal/mol). Seven additional phytochemicals: menthyl chavicol (-8.49 kcal/mol), bulnesol (-7.40 kcal/mol), cubebol (-7.34 kcal/mol), β-cubebene (-7.31 kcal/mol), guaiol (-7.27 kcal/mol), and (-)-β-bourbonene (-7.27 kcal/mol), also showed more favorable scores than meropenem (-7.28 kcal/mol). In contrast, gallic acid (-5.38 kcal/mol) displayed the least favorable XP score among the reported compounds.

The highly favorable score of Ocimol showed a combination of hydrogen-bonding (-1.91 kcal/mol) and lipophilic van der Waals (-6.01 kcal/mol) contributions, indicating that its strong overall score was not attributable solely to hydrophobic interactions. Ciprofloxacin also exhibited combined hydrogen-bonding (-0.96 kcal/mol), electrostatic (-0.40 kcal/mol), and lipophilic van der Waals (-4.57 kcal/mol) contributions. Meropenem showed a comparable interaction pattern, although with a less favorable overall score.

Most of the terpene-rich compounds, including menthyl chavicol, bulnesol, cubebol, β-cubebene, guaiol, (-)-β-bourbonene, β-guaiene, zizanene, γ-muurolene, and hedycaryol, exhibited negligible hydrogen-bond and electrostatic contributions but relatively favorable lipophilic van der Waals terms. This interaction profile is consistent with the physicochemical characteristics of the AcrB distal binding pocket, which is enriched in hydrophobic phenylalanine residues, particularly Phe136, Phe178, Phe610, Phe615, Phe617, and Phe628. Structural and mutational studies have established the importance of these residues in accommodating chemically diverse AcrB substrates through hydrophobic, van der Waals, and aromatic interactions.

Table 1: Glide XP Docking Scores of the Top-ranked *Ocimum gratissimum* Phytochemicals and Standard Antibiotics against AcrB

Ligand	XP GScore (kcal/mol)	H-bond term	Electrostatic term	Lipophilic vdW term
Ocimol	-10.71	-1.91	-0.32	-6.01
Ciprofloxacin (standard)	-10.19	-0.96	-0.40	-4.57
Menthyl chavicol	-8.49	0.00	0.01	-5.49
Bulnesol	-7.40	0.00	0.01	-4.36
Cubebol	-7.34	0.00	-0.03	-4.11
beta-Cubebene	-7.31	0.00	0.01	-4.12
Meropenem (standard)	-7.28	-1.05	-0.64	-3.27
Guaiol	-7.27	0.00	-0.07	-4.15
(-)-beta-Bourbonene	-7.27	0.00	0.01	-4.08
beta-Guaiene	-7.16	0.00	0.01	-3.96
Zizanene	-6.91	0.00	-0.01	-3.70
gamma-Muurolene	-6.91	0.00	-0.01	-3.70
Hedycaryol	-6.84	0.00	-0.07	-3.71
Gallic acid	-5.38	-2.40	-0.20	-2.02

ADMET Assay of the Ligands

The pharmacokinetic and toxicity profiling of the selected phytochemicals were evaluated using ADMETlab 3.0 to determine their potential absorption, distribution, metabolic, excretion and toxicity. The analysis includes human intestinal absorption (HIA), blood-brain barrier (BBB) permeability, CYP3A4 inhibition, hERG liability, Ames mutagenicity, drug-induced liver injury (DILI), and carcinogenicity predictions (Table 2). These parameters were considered alongside molecular docking results to distinguish compounds with favourable predicted target interactions from those exhibiting potentially undesirable properties (Fu *et al*., 2024). Significant divergence was observed in human intestinal absorption (HIA) models. Sesquiterpene hydrocarbons; particularly (−)-β-bourbonene (0.89) and β-guaiene (0.78), exhibited high transcellular permeation probabilities. Conversely, oxygenated analogs and menthyl chavicol yielded negligible calculated HIA values (5×10^{-7}),

bulnesol (0.0003), β-cubebene (0.004), γ-muurolene (0.008), and gallic acid (0.002), showed very low predicted HIA probabilities. Zizanene displayed an intermediate HIA prediction of 0.42. These differences indicate that the physicochemical characteristics of the phytochemicals may substantially influence their predicted absorption behaviour (Encinar *et al*., 2026).

The CYP3A4 inhibition profiles were generally favourable for most of the compounds. Zizanene exhibited an exceptionally low predicted probability of CYP3A4 inhibition (7×10^{-10}), followed by (-)-β-bourbonene (4×10^{-6}), β-guaiene (4×10^{-4}), and γ-muurolene (0.015). In contrast, bulnesol showed a markedly higher probability of CYP3A4 inhibition (0.85), representing a potential metabolic drug-drug interaction profile. The relatively low CYP3A4 inhibition probabilities observed for several candidates are desirable because inhibition of this major drug-metabolizing enzyme may alter the disposition of co-administered therapeutic agents (Fu *et al*., 2024), hERG analysis was generally low across the phytochemical candidates, with probabilities ranging from 0.04 to 0.13 for most compounds. β-guaiene exhibited particularly low predicted hERG liability (0.008), while (-)-β-bourbonene, zizanene, γ-muurolene, and Hedycaryol also showed relatively low probabilities. β-guaiene exhibited a notably high predicted Ames probability (0.95) and DILI probability (0.80), indicating potentially important mutagenic and hepatotoxic profiles despite its favourable predicted CYP3A4 and hERG profiles. Bulnesol similarly presented an unfavourable overall toxicity profile, with predicted CYP3A4 inhibition, Ames mutagenicity, and carcinogenicity probabilities of 0.85, 0.56, and 0.92, respectively. Cubebol and β-cubebene also showed relatively high carcinogenicity predictions (0.77 and 0.79, respectively), accompanied by moderately elevated Ames probabilities.

Among the investigated compounds, zizanene displayed one of the more balanced predicted profiles. It showed low predicted CYP3A4 inhibition (7×10^{-10}), hERG profile (0.08), DILI (0.07), and carcinogenicity (0.28), together with an intermediate HIA prediction (0.42). γ-Muurolene likewise demonstrated low predicted CYP3A4 inhibition (0.015), hERG profile (0.05), Ames mutagenicity (0.16), DILI (0.03), and carcinogenicity (0.15). However, its very low predicted HIA (0.008) represents a potential limitation if systemic oral exposure is required. Hedycaryol exhibited low predicted CYP3A4 inhibition (0.019), hERG profile (0.06), Ames probability (0.34), and DILI probability (0.08), although its carcinogenicity prediction (0.66) warrants caution. Gallic acid showed low predicted CYP3A4 inhibition (0.013), hERG profile (0.04), and DILI probability (0.10), but its low predicted HIA and moderate Ames and carcinogenicity probabilities suggest a mixed developability profile.

The reference antibiotics exhibited distinct computational profiles. In these models, meropenem displayed a high predicted HIA probability (0.93), whereas ciprofloxacin showed a substantially lower predicted value (0.002). These discrepancies highlight the applicability domain limitations of machine-learning models trained predominantly on conventional oral small-molecule libraries. In clinical settings, meropenem is restricted to parenteral delivery due to hydrolytic instability and polarity, whereas ciprofloxacin achieves approximately 70% human oral bioavailability via active and zwitterionic transport mechanisms not captured by passive permeability algorithms. Therefore, these computational values serve strictly as comparative *in silico* benchmarks rather than reflections of established clinical disposition.

Table 2: ADMET Profile of the Screened Phytochemicals and Standard Drugs

Compound	HIA	BBB	CYP3A4 inhib.	hERG	Ames	DILI	Carcinogenicity
Ocimol	0.001	0.980	0.000003	0.13	0.11	0.09	0.64
Menthyl chavicol	5×10^{-7}	0.04	0.16	0.08	0.11	0.04	0.39
Bulnesol	0.0003	0.31	0.85	0.05	0.56	0.23	0.92
Cubebol	0.009	0.04	0.26	0.06	0.45	0.13	0.77
β-Cubebene	0.004	0.62	0.23	0.08	0.55	0.24	0.79
Guaiol	0.002	0.11	0.21	0.23	0.00003	0.10	0.80
(-)-β-Bourbonene	0.89	0.27	0.000004	0.04	0.26	0.05	0.21
β-Guaiene	0.78	0.03	0.0004	0.008	0.95	0.80	0.18
Zizanene	0.42	0.09	7×10^{-10}	0.08	0.48	0.07	0.28
γ-Muurolene	0.008	0.004	0.015	0.05	0.16	0.03	0.15
Hedycaryol	0.11	0.04	0.019	0.06	0.34	0.08	0.66
Gallic acid	0.002	0.02	0.013	0.04	0.53	0.10	0.54
Ciprofloxacin	0.002	0.0009	4.6×10^{-9}	0.47	0.76	1.00	0.19
Meropenem	0.93	0.0001	0.025	0.02	0.51	1.00	0.12

Drug Likeness Analysis of the Selected Compounds

The physicochemical descriptors and drug-likeness criteria defined by Lipinski's Rule of Five (Ro5); molecular weight (≤ 500 g/mol), octanol-water partition coefficient, hydrogen bond donors (HBD ≤ 5), and hydrogen bond acceptors (HBA ≤ 10), were computed to evaluate the druglikeness properties of the selected *Ocimum gratissimum* phytochemicals alongside the reference antibiotics (Table 3) (El Zahed *et al*., 2021; Abdul-Hammed *et al*., 2024).

The vast majority of the selected phytochemicals strictly adhered to Lipinski's criteria, exhibiting zero violations. Monoterpenoids, aromatic ethers, and sesquiterpenoids; including menthyl chavicol, bulnesol, cubebol, β-cubebene, (−)-β-bourbonene, β-guaiene, zizanene, γ-muurolene, and hedycaryol, displayed molecular weights within the narrow, highly druggable range of 148.20 to 222.37 g/mol. Their calculated logP values fell between 3.10 and 4.80, reflecting moderate to high lipophilicity that remains beneath the threshold of 5.0. This lipophilic profile aligns closely with the energetic demands of the AcrB distal binding pocket. Because the hydrophobic trap and substrate translocation channel of the AcrB tight (T) protomer are dominated by aromatic residues (such as Phe136, Phe178, Phe610, Phe615, Phe617, and Phe628), modest lipophilicity (logP between 3.50 and 4.80) and structural rigidity favor non-covalent, dispersion-

driven van der Waals contacts without crossing the boundary into irreversible non-specific aggregation (Alenazy, 2022).

In contrast, the top docking candidate, ocimol, breached Lipinski's guidelines with two rule violations, driven by an elevated molecular weight of 620.87 g/mol and high lipophilicity with a logP of 6.80. While these extensive lipophilic surfaces explain its superior docking score of −10.71 kcal/mol through extensive hydrophobic entrapment, severe departures from Ro5 parameter space typically correlate with poor aqueous solubility and erratic oral bioavailability. However, modern antimicrobial and adjuvant discovery frameworks increasingly recognize that natural products and bacterial membrane or efflux modulators frequently occupy "beyond Rule of Five" (bRo5) chemical space. Even so, the dual Ro5 infractions of ocimol, coupled with its negligible predicted intestinal absorption of 0.001 (Table 2), suggest that structural optimization or nano-based delivery formulation would be mandatory if systemic administration were pursued.

Gallic acid also satisfied all Ro5 criteria (molecular weight of 170.12 g/mol, logP of 0.70, 4 hydrogen bond donors, and 5 hydrogen bond acceptors), but its highly hydrophilic and polar character produced poor lipophilic complementarity with the hydrophobic distal pocket, accounting for its comparatively weak docking energy of −5.38 kcal/mol. The reference therapeutics, ciprofloxacin and meropenem, also complied fully with the Rule of Five, exhibiting negative calculated logP values of −0.70 and −3.20, respectively, and higher polar atom densities. This hydrophilic disposition illustrates the fundamental chemical divergence between classical broad-spectrum antibiotics, which depend heavily on outer membrane porin permeation, and hydrophobic efflux pump inhibitors or resistance-modifying adjuvants, which competitively target the deep lipophilic grooves of the AcrB chamber to impede substrate extrusion. Among the zero-violation candidates that balanced both target affinity and safety parameters, zizanene (molecular weight of 204.35 g/mol, logP of 4.10, and zero violations) stands out. Its molecular compactness and lipophilic balance conform to the optimal physicochemical envelope required for small-molecule bacterial efflux modulators while avoiding the pharmacokinetic penalties seen with high-molecular-weight congeners.

Table 3: Drug-Likeness Properties of the Selected Compounds

Compound	MW (g/mol)	LogP	HBD	HBA	Ro5 Violations
Ocimol	620.87	6.80	1	6	2
Menthyl chavicol	148.20	3.10	0	1	0
Bulnesol	222.37	3.80	1	1	0
Cubebol	222.37	3.65	1	1	0
β-Cubebene	204.35	4.60	0	0	0
(-)-β-Bourbonene	204.35	4.70	0	0	0
β-Guaiene	204.35	4.80	0	0	0
Zizanene	204.35	4.10	0	0	0
γ-Muurolene	204.35	4.65	0	0	0
Hedycaryol	222.37	3.90	1	1	0
Gallic acid	170.12	0.70	4	5	0
Ciprofloxacin	331.34	-0.70	2	5	0
Meropenem	383.46	-3.20	4	8	0

Oral Bioavailability and Physicochemical Profiling

Following the drug-likeness screening, an extensive computational assessment of the oral bioavailability of the selected *Ocimum gratissimum* phytochemicals and standard antibiotics was conducted using the SwissADME web tool (Table 4). Although every evaluated ligand and reference control met the minimum threshold for gastrointestinal permeation; each meeting the requirement of an Abbott bioavailability score of 0.55, denoting a ≥ 55% probability of oral exposure, in-depth parsing of the individual continuous descriptors revealed marked mechanistic divergence in their predicted biophysical behavior (Ogbeide & Owowenu, 2026). Evaluation of topological polar surface area (TPSA) and conformational rotatable bond counts (NRotB) demonstrated that the majority of the natural constituents strictly complied with Veber's oral bioavailability criteria of TPSA ≤ 140 Å² and NRotB of ≤ 10. Pure sesquiterpenic hydrocarbons; specifically, β-cubebene, (−)-β-bourbonene, β-guaiene, zizanene, and γ-muurolene, presented non-polar surfaces with a TPSA = 0.00 Å² Å² and structural rigidity with zero rotatable bonds. This combination facilitates barrier-free passive transcellular partitioning across biological membranes, although it carries the potential trade-off of excessive lipophilic retention within membrane cores. Oxygenated analogues such as bulnesol, cubebol, guaiol, and hedycaryol displayed a modest polar footprint with a TPSA = 20.23 Å² and low conformational freedom with one rotatable bond, striking a balanced profile between polar desolvation penalties and membrane permeation kinetics. In contrast, gallic acid exhibited an elevated polar surface with a TPSA = 97.99 Å² despite its lower molecular weight of 170.12 g/mol, illustrating a high heteroatom density that impairs passive lipid bilayer crossing. The reference antibiotics ciprofloxacin (TPSA = 74.57 Å² and 3 rotatable bonds) and meropenem (TPSA = 114.45 Å² and 5 rotatable bonds) exhibited polar, flexible profiles typical of broad-spectrum hydrophilic antibacterials that enter Gram-negative envelopes via porin channels rather than passive lipophilic diffusion.

Table 4: Physicochemical Descriptors, Oral Bioavailability Properties, and Medicinal Chemistry Metrics of Prioritized *Ocimum gratissimum* Compounds and Reference Antibiotics

Compound	Formula	Glide XP Score (kcal/mol)	Mass (g/mol)	TPSA (A°2)	Rotatable Bonds	XLOGP3	WLOGP	ESOL logS	Ro5 Violations	Bioavailability Score	PAINS Alerts	Fraction Csp3	Synthetic Accessibility
Ocimol	$C_{40}H_{60}O_6$	-10.71	620.87	89.22	6	6.80	6.45	-6.45	2	0.55	0	0.75	6.85
Menthyl chavicol	$C_{10}H_{12}O$	-8.49	148.20	9.23	2	3.10	2.85	-2.35	0	0.55	0	0.20	1.85
Bulnesol	$C_{15}H_{26}O$	-7.40	222.37	20.23	1	3.80	3.60	-3.40	0	0.55	0	0.93	4.45
Cubebol	$C_{15}H_{26}O$	-7.34	222.37	20.23	0	3.65	3.52	-3.35	0	0.55	0	0.93	4.60
β - Cubebene	$C_{15}H_{24}$	-7.31	204.35	0.00	0	4.60	4.42	-4.15	0	0.55	0	0.87	4.25
Guaiol	$C_{15}H_{26}O$	-7.27	222.37	20.23	1	3.88	3.60	-3.42	0	0.55	0	0.93	4.38
(-)- *β* - Bourbonene	$C_{15}H_{24}$	-7.27	204.35	0.00	0	4.70	4.45	-4.18	0	0.55	0	0.87	4.80
β-Guaiene	$C_{15}H_{24}$	-7.16	204.35	0.00	0	4.80	4.52	-4.20	0	0.55	0	0.87	4.30
Zizanene	$C_{15}H_{24}$	-6.91	204.35	0.00	0	4.10	4.15	-3.85	0	0.55	0	0.87	4.20
γ - Muurolene	$C_{15}H_{24}$	-6.91	204.35	0.00	0	4.65	4.48	-4.12	0	0.55	0	0.87	4.22
Hedycaryol	$C_{15}H_{26}O$	-6.84	222.37	20.23	1	3.90	3.75	-3.45	0	0.55	0	0.93	4.35
Gallic acid	$C_7H_6O_5$	-5.38	170.12	97.99	1	0.70	0.59	-1.48	0	0.55	0	0.00	1.40
Ciprofloxacin	$C_{17}H_{18}FN$	-10.19	331.34	74.57	3	-0.70	-0.92	-3.10	0	0.55	0	0.35	3.12
Meropenem	$C_{17}H_{25}N_3$	-7.28	383.46	114.45	5	-3.20	-2.85	-1.85	0	0.55	0	0.47	4.85

Aqueous thermodynamic solubility (ESOL logS) alongside lipophilic partitioning (XLOGP3) further resolved the developability landscapes of the candidates. Menthyl chavicol, bulnesol, cubebol, guaiol, zizanene, and hedycaryol populated the desirable solubility-permeability window, yielding moderate-to-good predicted solubility (logS from −2.35 to −3.85) matched with Lipinski-compliant lipophilicity (XLOGP3 from 3.10 to 4.10). Conversely, β-cubebene, (−)-β-bourbonene, β-guaiene, and γ-muurolene approached the poorly soluble boundary (logS ≤ −4.12), driven by elevated lipophilicity (XLOGP3 from 4.60 to 4.80). Ocimol showed the most pronounced solubility penalty (logS of −6.45, XLOGP3 of 6.80), confirming that its strong docking energy of −10.71 kcal/mol is largely mediated by extensive hydrophobic entrapment within the phenylalanine-rich AcrB distal pocket. While highly potent *in silico*, ocimol's poor aqueous solubility and high lipophilicity present dissolution-rate limitations that would necessitate lipid-based or nano-carrier delivery systems in translational settings. Both clinical controls, ciprofloxacin and meropenem, exhibited favorable aqueous solubility (logS of −3.10 and −1.85, respectively), ensuring unhindered dissolution in biological fluids.

Stereochemical complexity; quantified by the fraction of sp3-hybridized carbons (Fsp3), revealed an advantage for the natural sesquiterpene scaffolds. All sesquiterpenoids displayed high three-dimensionality (Fsp3 from 0.87 to 0.93), which supports optimal spatial complementarity with the asymmetric, deep binding contours of the AcrB tight (T) protomer while avoiding the non-specific, flat aromatic stacking associated with planar molecules. By contrast, menthyl chavicol (0.20), gallic acid (0.00), and ciprofloxacin (0.35) were dominated by planar, aromatic systems. Importantly, none of the 12 natural phytochemicals triggered pan-assay interference compounds (PAINS) alerts (zero alerts), confirming that their predicted binding affinities are free from false-positive flags, colloidal aggregation, or non-specific chemical reactivity. Synthetic accessibility (SA) scores ranged from 1.40 to 1.85 for simple aromatics (gallic acid and menthyl chavicol) and 4.20 to 4.80 for the sesquiterpenoid group, confirming that these core scaffolds are synthetically tractable for downstream hit-to-lead derivatization. Among the prioritized natural products, zizanene demonstrated the most balanced overall profile, pairing zero Ro5 violations and zero PAINS alerts with favorable permeability (TPSA of 0.00 square Angstroms, zero rotatable bonds), manageable aqueous solubility (logS of −3.85), and moderate lipophilicity (XLOGP3 of 4.10). This structural balance supports its progression as an oral resistance-modifying adjuvant targeting the AcrB multidrug efflux pump.

Ligand Efficiency and Bioactivity Analysis

To normalize target binding affinity with respect to molecular size, ligand efficiency metrics; ligand efficiency (LE), size-independent ligand efficiency scale (LE-scale), fit quality (FQ), and ligand-efficiency-dependent lipophilicity (LELP), were calculated for the selected *Ocimum gratissimum* phytochemicals and standard antibiotics (Table 5) following established biophysical drug discovery frameworks (Hopkins *et al*., 2014). Standard molecular docking algorithms inherently favor bulkier scaffolds that establish multiple non-specific dispersion contacts within deep binding crevices; evaluating per-atom binding free energies is therefore essential to prevent molecular-weight-driven scoring biases (Schultes *et al*., 2020).

Table 5: Bioactivity Analysis of the Selected Compounds and Standards

Compound	ΔG (kcal/mol)	HA	LE (kcal/mol/HA)	LE-scale	FQ	logP (XLOGP3)	LELP
Ocimol	-10.71	46	0.233	0.200	1.165	6.80	29.18
Menthyl chavicol	-8.49	11	0.772	0.592	1.304	3.10	4.02
Bulnesol	-7.40	16	0.463	0.512	0.904	3.80	8.21
Cubebol	-7.34	16	0.459	0.512	0.896	3.65	7.95
β-Cubebene	-7.31	15	0.487	0.527	0.924	4.60	9.45
Guaiol	-7.27	16	0.454	0.512	0.887	3.88	8.55
(-)-β-Bourbonene	-7.27	15	0.485	0.527	0.920	4.70	9.69
β-Guaiene	-7.16	15	0.477	0.527	0.905	4.80	10.06
Zizanene	-6.91	15	0.461	0.527	0.875	4.10	8.89
γ-Muurolene	-6.91	15	0.461	0.527	0.875	4.65	10.09
Hedycaryol	-6.84	16	0.428	0.512	0.836	3.90	9.11
Gallic acid	-5.38	12	0.448	0.575	0.779	0.70	1.56
Ciprofloxacin	-10.19	24	0.425	0.404	1.052	-0.70	-1.65
Meropenem	-7.28	27	0.270	0.369	0.732	-3.20	-11.85

Note: ΔG represents the Glide XP GScore; HA denotes the heavy atom count; log P values are computed via XLOGP3.

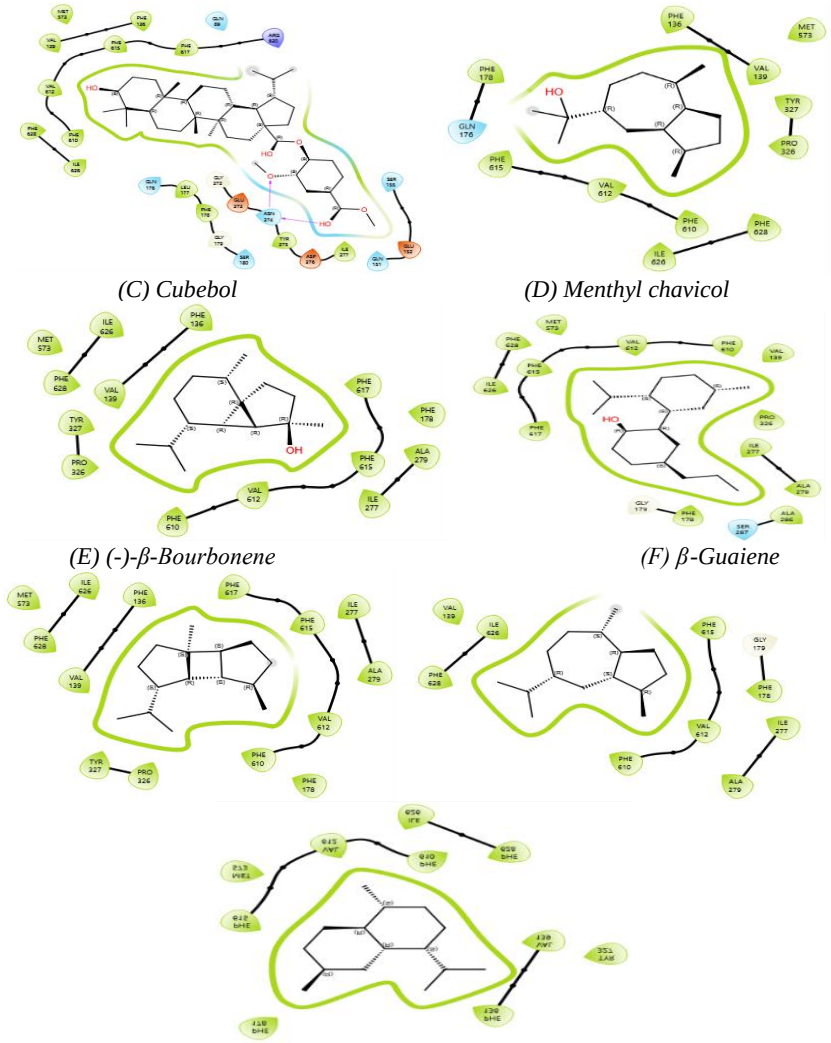
An acceptable requirement is a ligand efficiency of ≥ 0.30 kcal/mol/HA, with optimal geometrical binding fidelity designated by a fit quality value approaching unity (FQ approximately 1.0), which indicates near-maximal saturation of binding site contacts per unit volume (Reynolds *et al*., 2008). Menthyl chavicol exhibited an exceptionally high ligand efficiency of 0.772 kcal/mol/HA and fit quality of 1.304, which underscores the tight packing of its compact aromatic nucleus (11 heavy atoms) within the hydrophobic sub-cavities of the AcrB tight (T) protomer. Similarly, all evaluated sesquiterpenoids; comprising bulnesol, cubebol, β-cubebene, guaiol, (−)-β-bourbonene, β-guaiene, zizanene, γ-muurolene, and hedycaryol, surpassed the classic ligand efficiency benchmark (LE from 0.428 to 0.487 kcal/mol/HA) and exhibited fit quality indices close to the ideal ceiling (FQ from 0.836 to 0.924). These figures demonstrate that the compact carbobicyclic and carbotricyclic architectures of the sesquiterpene class engage the hydrophobic phenylalanine trap of AcrB (such as Phe136, Phe178, Phe610, and Phe628) with high steric and spatial efficiency. In sharp contrast, the top-docking hit ocimol failed to achieve the minimum efficiency cutoff (LE of 0.233 kcal/mol/HA). Although ocimol achieved an FQ of 1.165 relative to its size-dependent baseline (LE-scale of 0.200), its seemingly superior docking score of −10.71 kcal/mol is largely an artifact of its expanded molecular framework (46 heavy atoms), rather than exceptionally dense per-atom pharmacophoric contributions. Ciprofloxacin maintained strong atom profiles (LE of 0.425 kcal/mol/HA; FQ of 1.052), in keeping with its evolution as a targeted bacterial topoisomerase inhibitor, whereas meropenem showed a lower ligand efficiency (LE of 0.270 kcal/mol/HA; FQ of 0.732), consistent with its broad, hydrophilic, porin-dependent architectural design.

Evaluation of ligand-efficiency-dependent lipophilicity (LELP, defined as logP divided by LE) further distinguished candidates that achieve high-affinity binding through specific steric complementarity from those driven by non-specific, promiscuous hydrophobic partitioning. Drug discovery paradigms suggest that an optimal candidate maintains an LELP within the boundary of −10 to 10, as values exceeding 10 routinely correlate with elevated risks of rapid metabolic turnover, off-target promiscuity, and precipitation in aqueous media (Tarcsay & Keserű, 2013; Fu *et al*., 2024). Menthyl chavicol (LELP of 4.02) and gallic acid (LELP of 1.56) satisfied this criterion. Among the sesquiterpene derivatives, oxygenated members such as cubebol (7.95), bulnesol (8.21), and guaiol (8.55), along with the hydrocarbon zizanene (8.89), successfully remained below the critical threshold of 10.0, indicating that their target residence within the AcrB cavity is balanced by favorable shape matching rather than unchecked lipophilic drive. Conversely, β-cubebene (9.45) and (−)-β-bourbonene (9.69) skirted the upper limit, while β-guaiene (10.06) and γ-muurolene (10.09) marginally crossed the threshold, pointing to heavier lipophilic liabilities that mirror their predicted Ames and hepatotoxic flags observed during ADMET profiling. Ocimol displayed an unfavorable LELP of 29.18, substantially breaching acceptable medicinal chemistry boundaries and confirming that its binding interaction is dominated by extreme lipophilicity (XLOGP3 of 6.80). Synthesizing the ligand efficiency parameters alongside earlier ADMET and drug-likeness observations underscores zizanene as the most promising resistance-modifying lead candidate. With a favorable docking energy of −6.91 kcal/mol, robust atom profiles (LE of 0.461 kcal/mol/HA), near-ideal pocket fitting (FQ of 0.875), and a balanced lipophilicity-efficiency index (LELP of 8.89), zizanene presents a well-rounded biophysical and developability profile. It achieves effective engagement with the AcrB efflux pocket while circumventing the severe pharmacokinetic, solubility, and metabolic liabilities that constrain high-molecular-weight, excessively lipophilic congeners.

Molecular Binding Modes and Interaction Fingerprints within the AcrB Distal Binding Pocket

The molecular interactions and binding mode of the selected *Ocimum gratissimum* phytochemicals and clinical control antibiotics within the distal binding pocket of the AcrB tight (T) protomer (PDB ID: 4DX5) are detailed in Table 6, two-dimensional ligand–receptor interaction diagrams of the selected *Ocimum gratissimum* hits were systematically evaluated (Figure 2). Corroborating the Glide XP energetic scoring partitions (Table 1), the docked orientations illustrate two distinct mechanistic binding modalities: an extensive dual-anchor network characterized by simultaneous hydrogen-bonding and deep lipophilic entrapment observed for high-molecular-weight multi-ring scaffolds like ocimol, and an entropy-driven steric confinement within the aromatic "phenylalanine trap" shared across the compact sesquiterpene scaffolds.

(A) Ocimol *(B) Bulnesol*



(C) Cubebol *(D) Menthyl chavicol*

(E) (-)-β-Bourbonene *(F) β-Guaiene*

(G) γ-Muurolene

Figure 2: Two-Dimensional Ligand Interaction Diagrams of Prioritized Ocimum Gratissimum Phytochemicals Docked within the Distal Binding Pocket of the AcrB Tight (T) Protomer (PDB ID: 4DX5): (A) Ocimol, (B) Bulnesol, (C) Cubebol, (D) Menthyl Chavicol, (E) (-)-β-Bourbonene, (F) β-Guaiene, and (G) γ-Muurolene. Residues are Colored by Physicochemical Characteristics: Green (Hydrophobic), Light blue (polar), Orange (Negatively Charged), and Dark Blue (Positively Charged). Purple Directional Arrows Indicate Hydrogen-Bonding Interactions

The binding conformation of ocimol (Glide XP GScore: -10.71 kcal/mol; Figure 2A) reveals the structural basis of its top-ranking affinity. The extended pentacyclic triterpene backbone of ocimol spans the longitudinal axis of the hydrophobic distal channel, establishing extensive non-polar van der Waals contacts with Phe136, Phe178, Phe610, Phe615, Phe617, Phe628, Val139, Val612, Ile626, and Met573. This large hydrophobic contact area drives its dominant lipophilic van der Waals free energy term (-6.01 kcal/mol). Beyond hydrophobic packing, ocimol is securely anchored to the polar switch loop via directional hydrogen bonds; specifically, the hydroxyl and ether oxygen groups of its terminal substituted cyclohexyl moiety serve as reciprocal hydrogen-bond donor and acceptor partners with the carboxamide side chain of Asn274. Additional electrostatic stabilization is provided by proximal anionic residues Glu273, Asp276, and Glu152, alongside polar contacts with Ser155 and Ser180. These dual electrostatic and dispersion contacts bridge the flexible phenylalanine floor to the regulatory ceiling of the T protomer, stabilizing the local architecture and sterically hindering the conformational cycling required for functional drug extrusion (Eicher *et al*., 2012; Ruggerone *et al*., 2013). Conversely, the sesquiterpene candidates; bulnesol (-7.40 kcal/mol; Figure 2B), cubebol (-7.34 kcal/mol; Figure 2C), (-)-β-bourbonene (-7.27 kcal/mol; Figure 2E), β-guaiene (-7.16 kcal/mol; Figure 2F), and γ-muurolene (-6.91 kcal/mol; Figure 2G), alongside menthyl chavicol (-8.49 kcal/mol; Figure 2D), achieve stable pocket lodging primarily through shape-complementary steric packing within the hydrophobic core. Consistent with their negligible hydrogen-bonding energies (0.00 kcal/mol; Table 1), these scaffolds lack directed polar linkages to the protein backbone, nesting instead within the aromatic floor formed by Phe136, Phe178, Phe610, Phe615, Phe617, and Phe628, bounded by Val139, Val612, Ile626, Ile277, Pro326, and Met573. Bulnesol (Figure 2B) and cubebol (Figure 2C) orient their bicyclic and tricyclic carbon skeletons directly toward the Phe610-Val612-Phe615 motif. Although both chemical entities possess a single tertiary alcohol group, these hydroxyl substituents remain oriented toward solvent-accessible

boundaries or adjacent weakly polar residues (such as Gln176 in bulnesol) without forming classical donor–acceptor hydrogen bonds with the binding pocket. Their binding stability is maintained by steric confinement between Val139, Ile626, and Phe628. In cubebol, the fused cyclopropyl moiety embeds within the hydrophobic recess framed by Phe615, Phe617, and Ile277, complementing the surrounding aromatic architecture.

The pure hydrocarbon sesquiterpenes (-)-β-bourbonene (Figure 2E), β-guaiene (Figure 2F), and γ-muurolene (Figure 2G) occupy the central hydrophobic crevice through dispersion interactions driven by their non-polar frameworks TPSA = 0.00 Å². Their peripheral methyl and isopropyl substituents project into complementary hydrophobic recesses defined by Phe136, Val139, Phe610, Phe615, and Phe628. Residues Phe610, Val612, and Phe615 form a conserved contact triad across all three hydrocarbons, establishing an unbroken van der Waals contact layer across the base of the extrusion channel. Menthyl chavicol (Figure 2D) projects its alkyl-substituted cyclohexyl core into the deep sub-cavity bounded by Phe178, Phe615, Phe617, Val612, and Ile277. This structural fit accounts for its high ligand efficiency (LE = 0.772 kcal/mol/HA) and fit quality (FQ = 1.304), driven by favorable desolvation of its non-polar surface against Gly179 and Phe178. These structural patterns highlight the central role of the AcrB aromatic trap in substrate recognition. The distal pocket relies on its clustered phenylalanine side chains (Phe136, Phe178, Phe610, Phe615, Phe617, and Phe628) as a flexible hydrophobic switch that alters rotameric orientations to accommodate diverse lipophilic molecules. The predicted binding poses suggest that occupation of the phenylalanine-rich distal pocket by prioritized *Ocimum gratissimum* constituents could potentially interfere with substrate recognition, access by therapeutic antibiotics, or conformational dynamics; however, this mechanistic hypothesis requires molecular-dynamics and experimental validation. Accordingly, these phytochemical hits are best characterized as putative AcrB-binding scaffolds rather than confirmed competitive efflux pump inhibitors.

Table 6: Binding Mode and Detailed Molecular Interaction Profiles of the Prioritized *Ocimum gratissimum* Hits and Reference Antibiotics within the AcrB Distal Binding Pocket (PDB ID: 4DX5)

Ligand	XP GScore (kcal/mol)	H-Bond Partner(s)	Key Hydrophobic / vdW Contacts	Electrostatic / Other Contacts
Ocimol	-10.71	Asn274	Phe136, Phe178, Val139, Tyr275, Ile277, Met573, Phe610, Val612, Phe615, Phe617, Ile626, Phe628	Glu152, Glu273, Asp276 (electrostatic); Ser155, Ser180, Gln89, Gln151, Gln176 (polar); Arg620 (cationic)
Menthyl chavicol	-8.49	None	Phe178, Phe610, Phe615, Phe617, Val139, Val612, Ile277, Ala279, Ala286, Pro326, Met573, Ile626, Phe628	Gly179 (vdW backbone); Ser287 (polar)
Bulnesol	-7.40	None	Phe136, Val139, Phe178, Pro326, Tyr327, Met573, Phe610, Val612, Phe615, Ile626, Phe628	Gln176 (polar contact)
Cubebol	-7.34	None	Phe136, Val139, Phe178, Ile277, Ala279, Pro326, Tyr327, Met573, Phe610, Val612, Phe615, Phe617, Ile626, Phe628	None
(-)- β - Bourbonene	-7.27	None	Phe136, Val139, Phe178, Ile277, Ala279, Pro326, Tyr327, Met573, Phe610, Val612, Phe615, Phe617, Ile626, Phe628	None
β-Guaiene	-7.16	None	Val139, Phe178, Gly179, Ile277, Ala279, Phe610, Val612, Phe615, Ile626, Phe628	None
γ-Muurolene	-6.91	None	Phe136, Val139, Phe178, Tyr327, Met573, Phe610, Val612, Phe615, Ile626, Phe628	None
Ciprofloxacin *(SD1, reference)*	-10.19	Phe178, Gln151 Glu152	Ala279, Val612, Phe610, Ile277, Asn274, Ala286	Ser155, Ser287 (polar); Glu152 (electrostatic)
Meropenem *(SD2, reference)*	-7.28	Gln176, Leu177 Gly179, Phe610	Phe136, Val139, Pro326, Tyr327, Met573, Phe610, Val612, Phe615, Ile626, Phe628	

CONCLUSION

This investigation provides a comprehensive *in silico* biophysical and pharmacokinetic characterization of *Ocimum gratissimum* phytochemicals targeting the AcrB multidrug efflux pump in Escherichia coli by systematically integrating Glide Extra Precision docking, non-covalent binding topologies, ADMET profiling, Lipinski drug-likeness, oral bioavailability modeling, and ligand efficiency metrics. Structural analyses indicate that O. gratissimum terpenes engage the AcrB distal pocket through distinct non-covalent interactions: high-molecular-weight scaffolds such as ocimol bridge the hydrophobic floor to the polar regulatory ceiling via Asn274, whereas compact sesquiterpenoids primarily embed within the core aromatic phenylalanine trap formed by Phe136, Phe178, Phe610, Phe615, Phe617, and Phe628. These predicted binding orientations suggest that lodging within the phenylalanine trap could potentially interfere with

substrate access or pocket dynamics; however, this structural hypothesis requires dynamic and functional verification.

Normalizing docking scores by per-atom and lipophilicity contributions proved essential for separating genuine lead candidates from lipophilic scoring artifacts. Although ocimol achieved the most favorable absolute docking score of −10.71 kcal/mol, its elevated lipophilicity with a logP of 6.80, sub-threshold ligand efficiency of 0.233 kcal/mol per heavy atom, unfavorable lipophilicity index of 29.18, and negligible predicted intestinal absorption of 0.001 highlight substantial developability liabilities. In contrast, zizanene was computationally prioritized as the most balanced lead candidate, pairing a docking score of −6.91 kcal/mol with complete Lipinski compliance, zero PAINS alerts, robust ligand efficiency of 0.461 kcal/mol per heavy atom, a fit quality of 0.875, an acceptable lipophilic efficiency of 8.89, and a favorable computational toxicity profile devoid of prominent cardiotoxic or hepatotoxic flags.

These findings must be interpreted within the methodological boundaries of an *in silico* study. Molecular docking utilizes a static receptor conformation that does not simulate the continuous peristaltic rotation of the asymmetric AcrB trimer from the tight to open states, empirical docking scores provide relative scoring estimates rather than experimental thermodynamic free energies, and machine-learning ADMET predictions carry inherent applicability domain constraints. Consequently, these phytochemical hits represent putative AcrB-binding scaffolds rather than confirmed efflux pump inhibitors. Future investigations must prioritize atomistic molecular dynamics simulations, in vitro checkerboard microdilution assays to determine fractional inhibitory concentration indices with ciprofloxacin and meropenem, and real-time fluorometric dye-accumulation assays to experimentally determine whether zizanene can functionally inhibit bacterial efflux and restore antibiotic susceptibility.

ACKNOWLEDGEMENTS

The authors have no specific acknowledgements to declare

Conflict of Interest

The authors declare no conflict of interest

Funding

The authors received no specific funding for this research

REFERENCES

Abdul-Hammed, M., Adedotun, I., Ismail, U., Ayankoso, S., Abdul-razaq, R., Olajide, M. & Lawal, T. (2024). Investigating the bioactive compounds from *Capsicum annum* as a probable alternative therapy for prostate cancer treatment: a structure-based drug design approach. *Pure and Applied Chemistry*, *96*(5), 719-742. https://doi.org/10.1515/pac-2023-1111

Achuenu, C., Tanko, S., Nworie, M. O., Edah, A. O., & Adelakun, E. A. (2026). Analgesic activity, phytochemical profiling and toxicity assessment of ethanol extract from *Ocimum gratissimum* leaves cultivated in Jos, Nigeria. *FUDMA Journal of Sciences*, *10*(5), 249-255.

Alenazy, R. (2022). Drug efflux pump inhibitors: A promising approach to counter multidrug resistance in Gram-negative pathogens by targeting AcrB protein from AcrAB-TolC multidrug efflux pump from *Escherichia coli*. *Biology*, *11*(9), 1328. https://doi.org/10.3390/biology11091328

Baell, J. B., & Holloway, G. A. (2010). New substructure filters for removal of pan assay interference compounds (PAINS) from screening libraries and for their exclusion in bioassays. *Journal of Medicinal Chemistry*, *53*(7), 2719–2740. https://doi.org/10.1021/jm901137j

Brenk, R., Schipani, A., James, D., Krasowski, A., Gilbert, I. H., Frearson, J., & Wyatt, P. G. (2008). Lessons learnt from assembling screening libraries for drug discovery for neglected diseases. *ChemMedChem*, *3*(3), 435–444. https://doi.org/10.1002/cmdc.200700139

Chambial, P., Thakur, N., Bhukya, P. L., Subbaiyan, A., & Kumar, U. (2025). Frontiers in superbug management: Innovating approaches to combat antimicrobial resistance. *Archives of Microbiology*, *207*(3), 60. https://doi.org/10.1007/s00203-025-04262-x

Chetri, S., Bhowmik, D., Paul, D., Pandey, P., Chanda, D. D., Chakravarty, A., Bora, D., & Bhattacharjee, A. (2019). AcrAB-TolC efflux pump system plays a role in carbapenem non-susceptibility in *Escherichia coli*. *BMC Microbiology*, *19*(1), 210. https://doi.org/10.1186/s12866-019-1589-1

Daina, A., Michielin, O., & Zoete, V. (2017). SwissADME: A free web tool to evaluate pharmacokinetics, drug-likeness and medicinal chemistry friendliness of small molecules. *Scientific Reports*, *7*, 42717. https://doi.org/10.1038/srep42717

dos Santos, C. A. L., da Silva Pereira, R. L., Pereira-de-Morais, L., Santos, G. J. G., Coutinho, H. D. M., da Cunha, F. A. B., Rodrigues, F. F. G., de Sousa Júnior, D. L., & Silva, J. C. (2025). Antibacterial activity of ethanolic extract of *Ocimum gratissimum* L. (basil) and its toxicity against *Drosophila melanogaster*. *Pharmacological Research–Natural Products*, *7*, 100212.

Eicher, T., Cha, H., Seeger, M. A., Brandstätter, L., El-Delik, J., Bohnert, J. A., Kern, W. V., Verrey, F., Grütter, M. G., Diederichs, K., & Pos, K. M. (2012). Transport of drugs by the multidrug transporter AcrB involves an access and a deep binding pocket that are separated by a switch-loop. *Proceedings of the National Academy of Sciences*, *109*(15), 5687–5692. https://doi.org/10.1073/pnas.1114944109

El Zahed, S. S., French, S., Farha, M. A., Kumar, G., & Brown, E. D. (2021). Physicochemical and structural parameters contributing to the antibacterial activity and efflux susceptibility of small-molecule inhibitors of *Escherichia coli*. *Antimicrobial Agents and Chemotherapy*, *65*(4), e01925-20. https://doi.org/10.1128/AAC.01925-20

Encinar, J. A., Yang, C., Fernández-Ginés, R., Tang, Y., & Cuadrado, A. (2026). ADMET-driven chemical navigability rules for early-stage virtual compound prioritization. *Journal of Chemical Information and Modeling*, *66*(15), 9429–9447. https://doi.org/10.1021/acs.jcim.6c01901

Friesner, R. A., Murphy, R. B., Repasky, M. P., Frye, L. L., Greenwood, J. R., Halgren, T. A., Sanschagrin, P. C., & Mainz, D. T. (2006). Extra precision Glide: Docking and scoring incorporating a model of hydrophobic enclosure for protein-ligand complexes. *Journal of Medicinal Chemistry*, *49*(21), 6177–6196. https://doi.org/10.1021/jm051256o

Fu, L., Shi, S., Yi, J., Wang, N., He, Y., Wu, Z., Peng, J., Deng, Y., Wang, W., Wu, C., Lyu, A., Zeng, X., Zhao, W., Hou, T., & Cao, D. (2024). ADMETlab 3.0: An updated comprehensive online ADMET prediction platform enhanced with broader coverage, improved performance, API functionality and decision support. *Nucleic Acids Research*, *52*(W1), W422–W431. https://doi.org/10.1093/nar/gkae236

Hopkins, A. L., Groom, C. R., & Alex, A. (2004). Ligand efficiency: A useful metric for lead selection. *Drug Discovery Today*, *9*(10), 430–431. https://doi.org/10.1016/S1359-6446(04)03069-7

Hopkins, A. L., Keserü, G. M., Leeson, P. D., Rees, D. C., & Reynolds, C. H. (2014). The role of ligand efficiency metrics in drug discovery. *Nature Reviews Drug Discovery*, *13*(2), 105–121. https://doi.org/10.1038/nrd4163

Irekeola, A. A., Shueb, R. H., Abd Rahman, E. N. S. E., Afolabi, H. A., Wada, Y., Elmi, A. H., Hakami, M. A., Alghzwani, S. M., Elnoubi, O. A., & Alshehri, A. A. (2024). High prevalence of carbapenem-resistant Enterobacterales (CRE) in human samples from Nigeria: A systematic review and meta-analysis. *Heliyon*, *10*(15), e34926. https://doi.org/10.1016/j.heliyon.2024.e34926

Kim, H. Y., Kim, M.-S., & Shin, D. H. (2025). A study of flavonoid inhibitors against Monkeypox H1 phosphatase. *Journal of Enzyme Inhibition and Medicinal Chemistry*, *40*(1), 2535585. https://doi.org/10.1080/14756366.2025.2535585

Lipinski, C. A., Lombardo, F., Dominy, B. W., & Feeney, P. J. (2001). Experimental and computational approaches to estimate solubility and permeability in drug discovery and development settings. *Advanced Drug Delivery Reviews*, *46*(1–3), 3–26. https://doi.org/10.1016/S0169-409X(00)00129-0

Lomovskaya, O., Warren, M. S., Lee, A., Gallegos, A., Villegas, A., Donskey, C. J., & Watkins, W. (2001). Inhibition of efflux pumps as a novel approach to combat multidrug resistance in Gram-negative pathogens. *Journal of Antimicrobial Chemotherapy*, *47*(4), 461–466.

Lu, C., Wu, C., Ghoreishi, D., Chen, W., Wang, L., Damm, W., Ross, G. A., Dahlgren, M. K., Russell, E., von Bargen, C. D., Abel, R., Farid, R., & Harder, E. D. (2021). OPLS4: Improving force field accuracy on challenging regimes of medicinal chemistry space. *Journal of Chemical Theory and Computation*, *17*(7), 4291–4300. https://doi.org/10.1021/acs.jctc.1c00302

Mohanraj, K., Karthikeyan, B. S., Vivek-Ananth, R. P., Chand, R. P. B., Aparna, S. R., Mangalapandi, P., & Samal, A. (2018). IMPPAT: A curated database of Indian medicinal plants, phytochemistry and therapeutics. *Scientific Reports*, *8*, 4329. https://doi.org/10.1038/s41598-018-22631-z

Nakashima, R., Sakurai, K., Yamasaki, S., Hayashi, K., & Nishino, K. (2011). Structures of the multidrug exporter AcrB reveal a proximal multisite drug-binding pocket. *Nature*, *480*(7378), 565–569. https://doi.org/10.1038/nature10641

Odede, K. R., & Okesanya, O. J. (2024). Prevalence, antimicrobial susceptibility, and phenotypic identification of ESBL and carbapenemase-producing *Escherichia coli* from isolates of patients attending Edo Specialist Hospital, Nigeria. *Microbes and Infectious Diseases*.

Ogbeide, U. M., & Owowenu, K. O. (2026). In silico antihypertensive potential of phytoconstituents in indigenous leafy vegetables black soup of *Vernonia amygdalina* (bitter leaf), *Ocimum gratissimum* (scent leaf), and *Piper guineense* (uziza) in Edo State, Nigeria. *Journal of Applied Sciences & Environmental Management*, *30*(5), 1525.

Olsson, M. H. M., Søndergaard, C. R., Rostkowski, M., & Jensen, J. H. (2011). PROPKA3: Consistent treatment of internal and surface residues in empirical pKa predictions. *Journal of Chemical Theory and Computation*, *7*(2), 525–537. https://doi.org/10.1021/ct100578z

Opperman, C. H., Kwasny, S. M., Kim, H. S., Nguyen, S. T., O'Rourke, J. F., & Peet, N. P. (2014). Arylpiperazines as inhibitors of the AcrAB-TolC efflux pump of *Escherichia coli*. *Antimicrobial Agents and Chemotherapy*, *58*(2), 722–733.

Qin, W., Wang, H., Lv, K., Liu, S., Ma, T., Sang, S., & Chen, Y. (2026). Global burden of antimicrobial resistance in lower respiratory infections: A systematic analysis for the Global Burden of Disease Study 2021. *International Journal of Antimicrobial Agents*, *67*(6), 107786. https://doi.org/10.1016/j.ijantimicag.2026.107786

Reynolds, C. H., Tounge, B. A., & Bembenek, S. D. (2008). Ligand binding efficiency: Trends, physical basis, and implications. *Journal of Medicinal Chemistry*, *51*(8), 2432–2438. https://doi.org/10.1021/jm701255b

Reynolds, C. H., Tounge, B. Y., & Bembenek, S. D. (2008). Ligand-efficiency-dependent lipophilicity (LELP) as a guide in lead optimization. *ChemMedChem*, *3*(1), 74–77. https://doi.org/10.1002/cmdc.200700280

Ruggerone, P., Murakami, S., Pos, K. M., & Vargiu, A. V. (2013). RND efflux pumps: Structural information translated into function and inhibition mechanisms. *Current Topics in Medicinal Chemistry*, *13*(24), 3079–3100. https://doi.org/10.2174/15680266113136660220

Sastry, G. M., Adzhigirey, M., Day, T., Annabhimoju, R., & Sherman, W. (2013). Protein and ligand preparation: Parameters, protocols, and influence on virtual screening enrichments. *Journal of Computer-Aided Molecular Design*, *27*(3), 221–234. https://doi.org/10.1007/s10822-013-9644-8

Schultes, S., de Graaf, C., Haaksma, E. E. J., de Esch, I. J. P., Leurs, R., & Krämer, O. (2020). Ligand efficiency metrics in drug discovery: The pros and cons from a practical perspective. *Drug Discovery Today*, *25*(6), 1012–1026.

Sekar, P., Mamtora, D., Bhalekar, P., & Krishnan, P. (2022). AcrAB-TolC efflux pump mediated resistance to carbapenems among clinical isolates of Enterobacteriaceae. *Journal of Pure & Applied Microbiology*, *16*(3), 1982–1988.

Shelley, J. C., Cholleti, A., Frye, L. L., Greenwood, J. R., Timlin, M. R., & Uchimaya, M. (2007). Epik: A software program for pKa prediction and protonation state generation for drug-like molecules. *Journal of Computer-Aided Molecular Design*, *21*(12), 681–691. https://doi.org/10.1007/s10822-007-9134-9

Ugbogu, O. C., Emmanuel, O., Agi, G. O., Ibe, C., Ekweogu, C. N., Ude, V. C., Uche, M. E., Nnanna, R. O., & Ugbogu, E. A. (2021). A review on the traditional uses, phytochemistry, and pharmacological activities of clove basil (*Ocimum gratissimum* L.). *Heliyon*, *7*(11), e08404. https://doi.org/10.1016/j.heliyon.2021.e08404

Veber, D. F., Johnson, S. R., Cheng, H.-Y., Smith, B. R., Ward, K. W., & Kopple, K. D. (2002). Molecular properties that influence the oral bioavailability of drug candidates. *Journal of Medicinal Chemistry*, *45*(12), 2615–2623. https://doi.org/10.1021/jm020017n

Westermaier, Y. (n.d.). *In silico pharmacology in drug discovery: Methods for binding affinity prediction, identifying*. Retrieved September 9, 2026, from https://access.archive-ouverte.unige.ch/access/metadata/233cb277-5f06-4215-9816-eab9fd081671/download

Xiong, G., Wu, Z., Yi, J., Fu, L., Yang, Z., Hsieh, C., Yin, M., Zeng, X., Wu, C., Lu, A., Chen, X., Hou, T., & Cao, D. (2021). ADMETlab 2.0: An integrated online platform for accurate and comprehensive predictions of ADMET properties. *Nucleic Acids Research*, *49*(W1), W5–W14. https://doi.org/10.1093/nar/gkaa1000

Zeb, S., Nazir, A., Hameed, M. F., Ikram, S., Haider Naqvi, S. Z., Shoaib, M., Butaye, P., Wang, Z., Li, R., & Lu, X. (2026). Colistin resistance in Gram-negative bacteria: Mechanisms, transmission, and novel intervention strategies. *Microorganisms*, *14*(1), 173. https://doi.org/10.3390/microorganisms14010173

Zhou, H., Du, J., Jia, M., Li, Y., & Zheng, K. (2026). Medicinal plants: A promising therapeutic approach for addressing antimicrobial resistance. *International Journal of Molecular Sciences*, *27*(11), 4804. https://doi.org/10.3390/ijms27114804

Zwama, M., Kuroda, T., Mogi, T., Mizushima, T., & Tsuchiya, T. (2018). Structural basis of non-substrate recognition by the multidrug efflux pump AcrB. *Nature Communications*, *9*, 322.

©2026 This is an Open Access article distributed under the terms of the Creative Commons Attribution 4.0 International license viewed via https://creativecommons.org/licenses/by/4.0/ which permits unrestricted use, distribution, and reproduction in any medium, provided the original work is cited appropriately.